SYNTHESIS OF GOLD-AMINE NANOPARTICLES OF VARIOUS SIZES USING TWO DIFFERENT METHODS

by

YIJUN SUN

B.A., Jiangnan University, 2010

A THESIS

submitted in partial fulfillment of the requirements for the degree

MASTER OF SCIENCE

Department of Chemistry

College of Arts and Sciences

KANSAS STATE UNIVERSITY

Manhattan, Kansas

2012

Approved by:
Major Professor
Kenneth J. Klabunde

Abstract

The motivation for the preparation of gold nanoparticles includes their potential utility in sensors, nanoelectronics, and the vast basic knowledge we can gain from these novel materials. Colloids of gold nanoparticles are also one of the most stable and easiest to manipulate. Synthesizing gold nanoparticles with narrow size distribution, uniform shape, and good crystalline nature represents a significant challenge.

Thiols were found to be very efficient capping ligands for the digestive-ripening process in our research group, during which a colloidal suspension in a solvent is refluxed at the solvent boiling temperature in the presence of a capping ligand to convert a highly polydispersed colloid into a nearly monodispersed one.

The current thesis research focuses on using amines instead of thiols as the capping ligands, which were also found to have similar efficiency for this purpose. The major part of the work is devoted to understanding the digestive ripening of gold-amine colloids system, and the effect of the nature of the amine ligands.

A noteworthy achievement of the current work is the ability to synthesize stable gold colloids with different sizes by using different amine ligands. A diverse set of instrumental techniques is used for the characterization of the gold nanoparticles

Table of Contents

Table of figures

Acknowledgements

First and foremost, I would like to acknowledge my major professor, Dr. Klabunde, for providing me such a great opportunity to study and work in his lab, and also for his support in completing my master degree. Then, I would like to thank my lab mates, Manindu N Weerasinghe, Khadga Shrestha, Dambar Hamal and Yenting Kuo, they are always sharing their new ideas and were very helpful in the lab. In particular, I would like to thank Dr. Jose, who helped me the most in improving my experimental skills and always care about me.

I would also like to thank my committee members, Dr. Chris Sorensen and Dr. Jun Li for giving me insightful advice on my research, and the others in the Kansas State University Chemistry Department.

Finally, I would like to show my appreciation for my lovely friends, Yue Qi, Shuo Zeng, Yijing Li, David Lehman, Kelly French and Amber Wheeler, for their love and support. It is them that have kept me going through all the difficulties and not being lost on the way.

Dedication

This work is dedicated to my parents, for their endless love and great guidance on my life.

Chapter 1. Introduction and significance

The study of gold colloids has been one of the most ancient subjects of investigation in science. Since ancient Roman times, colloidal gold has been used to color glass intense shades of yellow, red, or purple, by changing the concentration of the gold. Modern scientific evaluation of gold colloids did not start until the marvelous work by Michael Faraday in 1857,[1] by whom the first colloidal gold synthesis method was reported. After that discovery, numerous researchers have investigated the unique properties of gold nanoparticles.[2] They are the most stable metal nanoparticles, presenting fascinating aspects such as individual particle behavior, electronic, magnetic and optical properties, as well as their wide application to catalysis and materials science.

1.1 Synthesis and Assembly

1.1.1 Review of Colloidal Synthesis Routes

Numerous methods for synthesis of gold colloids have been reported.[2] In general, two strategies can be distinguished, the bottom-up strategy and the top-down strategy.

The bottom-up strategy includes reduction of gold(III) salts in the presence of different stabilizing agents in solution. The most famous synthesis route for a long time has been that using citrate reduction of tetrachloroaurate ions in water, which was first conducted by Turkevitch in 1951.[3] It can easily achieve functionalization of the gold nanoparticle with water-soluble capping ligands and give particle core size of ca. 20 nm, but the control over the particle monodispersity is rather poor. Using alkanethiols to stabilize gold nanoparticles was first reported in 1993 by Mulvaney and Giersig. They first introduced thiols of different chain length as the capping ligands, which can strongly bind gold due to the soft character of both Au and S.[4] Inspired by this and Faraday's two-phase system[1], the most popular Brust-Schiffrin method for Au nanoparticles synthesis was conducted and reported in 1994,[5] which is another milestone in the overall field. It showed the possibility to synthesize thermally stable gold nanoparticles with narrowed dispersity and controlled size, and those nanoparticles can be repeatedly isolated and redissolved in organic solvents just like common chemicals. It was obtained by reducing tetrachloroaurate ions with sodium borohydride in the presence of thiols and a phase transfer agent,

tetraoctylammoniumbromide (TOAB). However, one reported disadvantage is the contamination of isolated gold nanoparticles with excess TOAB. To avoid using the phase transfer agent, recently several single-phase syntheses have been reported.[6-8] One involves reducing gold salts in aqueous (water/methanol) solution in the presence of water-soluble ligands.[9,10] Another employs the reduction with borohydrides ($LiBH_4$) that are soluble in the organic solvent (THF).

Except for reducing gold (III) to gold (0) by these chemical methods, there also emerged several physical methods: Photochemistry,[11-13] Sonochemistry,[14-16] Radiolysis,[17,18] and Thermolysis.[19,20] They basically dissolve gold salts in solution in the presence of some stabilizer, by employing extreme conditions, like UV irradiation, near-IR laser irradiation, high intensity ultrasound, specific radicals, etc., to control the gold nanoparticle sizes and improve the quality of particles.

The advantages of all of these bottom-up methods in the solution are (a) the possibility of controlling the particle size and dispersity by changing the reaction conditions (reaction time and temperature, as well as the reaction speed), and (b) producing the gold nanoparticles capped by various of functionalized ligands, and (c) simply to get isolated nanoparticles. While on the other hand, there are also some problems with these methods, such as (a) it's difficult to remove the impurities that are introduced to the process, like the extra surfactants, the reducing agents as well as the metal salts, and (b) it's hard to meet the requirements for scaling up from bench scale to industrial scale, presenting a number of reaction conditions, equipment design, and technology risks.

As for the top-down strategy, there are several ways to create gold clusters from bulk gold, including both attrition and pyrolysis. In attrition, the bulk gold can be ground into macro or micro scale particles by some size reducing mechanism, which usually can not give nano scale particles and the particle size are poly-dispersed. In pyrolysis, the bulk metal can be heated to atoms and re-form nano scale clusters. Specifically, in the Physical Vapor Deposition, the source metal will be thermally heated to atoms under an inert atmosphere and then those cooled metal atoms deposited on a cold finger to form metal clusters. When the process is finished, the metal clusters can be collected by removing them from the cold finger.[21] The Solvated Metal Atom Dispersion (SMAD) technique was first developed by Klabunde et al.[22-25] in 1979, which had a significant effect on the whole nano material field for more than a decade because it showed the possibility of synthesizing

pure gold nanoparticals on a large scale to make the functionalized gold nanoparticles being used in commercial application.

As we discussed, compared with the bottom-up strategy, the major advantages of the top-down strategy are obtaining size controlled and stabilized metal nanoparticles without any impurities, as well as scaling up the process for industrial application. However, the primary disadvantage lies in the restricted capping ligands which require stronger interactions between metal and capping ligands.

1.1.2 Specific methods for gold nanoparticles

1.1.2.1 Inverse Micelle Method

The inverse micelle method provides the preparation of metal colloidal particles (e.g. gold, palladium, silver, rhodium, nickel, iron, platinum) or colloidal alloy particles (silver/iridium or platinum/gold). Typically, an inverse micelle solution of a metal salt is first formed by dissolving a surfactant and the metal salt in an organic solvent. The surfactant molecule contains a hydrophilic head and a hydrophobic tail, so those molecules order themselves into spherical inverse micelle separating the aqueous and organic phases. The metal salt will stay inside of the inverse micelles in the aqueous phase. Then it is reduced to metal colloidal particles by adding the reducing agent. The size and number of inverse micelles is controlled by changing the concentration of the surfactant, which also determines the size of the elemental metal particles and their size distribution. Another metal salt can be added with further reduction to form the colloidal alloy particles. After the metal colloids are formed, the two-phase homogeneous solution can be dissolved again into another solvent, in which the metal nanoparticles have low dissolubility. Then the metal particles can be separated and dried to form a powder that is ready to use. Figure 1.1 represents a schematic overview of a typical inverse micelle method (Didodecyl dimethyl ammonium bromide (DDAB)).[26]

Figure 1.1

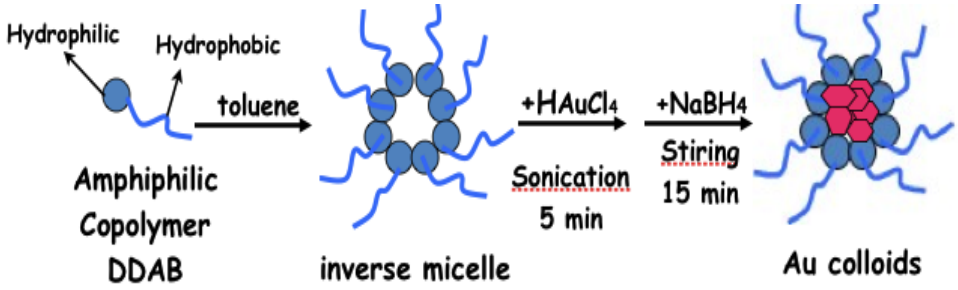

Figure 1.1 The schematic overview of the inverse micelle synthesis procedure

1.1.2.2 Solvated Metal Atom Dispersion (SMAD) Method

The SMAD technique was first reported by Klabunde and co-workers for the preparation of thiol capped gold colloids.[27] Since then, a variety of metal colloids (silver, copper, magnesium, and palladium) have been synthesized by SMAD in our laboratory.[24, 28] Compared with the inverse micelle and other methods, the major advantage of the SMAD technique is that it can yield pure metal colloids without any byproducts. Also it can provide wide industrial applications by scaling up the process to guarantee the products in large amounts and with reproducible quality.

Figure 1.2 shows a sketch of the SMAD setup. It contains several parts: the solvent Schlenk tube, the bridge head, the shower head, the electrodes and the reactor. Inside the reactor, the two water cooled copper electrodes are connected by the crucible, where the metal will be placed. The temperature is required to reach high enough to evaporate the bulk metal. On top of the reactor the bridge head connects the Schlenk tube and shower head; when vacuum is applied, the vapor of the solvent will come through the shower head and co-condense with the metal atoms on the walls of the reactor cooled to 77K. After the warming up stage, the matrix is melted down and stirred with the capping ligand at the bottom of the reactor. The particles are stabilized both sterically (by solvation) and electrostatically (by incorporation of a negative charge).

Figure 1.2

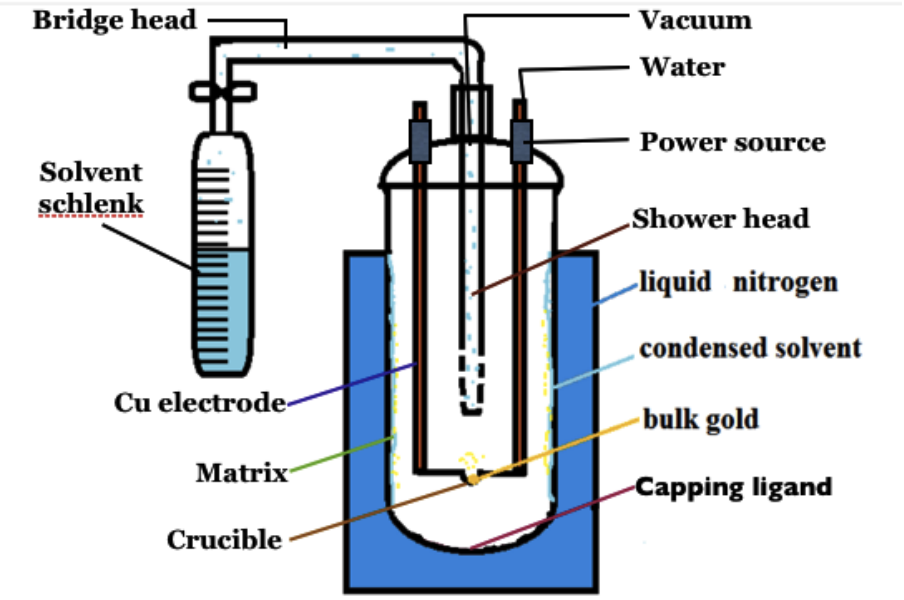

Figure 1.2 The SMAD setup

1.2 Capping ligands

The capping ligands play an important part in controlling the size, shape, and interparticle separation of the metal nanoparticles. The most popular capping ligands for gold nanoparticles are the alkanethiols. The thiol-capped gold nanoparticles are nonpolar and with core diameter of 1-4 nm, which have been extensively studied and reported covering a wide range of morphological, optical, electric, physical and chemical aspects,[29-36] Various other ligands capped gold nanoparticles have also been prepared through a two-phase synthesis process. The list includes amines, phosphines, carboxylates, polymers, dendrimers, and bio-functionalized molecules.[37, 38]

The gold-ligand interactions may be explained by the hard and soft acid-base theory, which states that a soft acid-like gold cluster prefers to interact with a softer base such as RSH and RNH2, rather than hard bases such as ROH. As mentioned before, the SMAD technique was first reported by Klabunde and co-workers for the preparation of thiol capped gold colloids.[27] Since then, a variety of metal colloids (silver, copper, magnesium, and palladium) have been synthesized by this method.[28-29] Compared with the inverse micelle and other methods, the major advantage of the

SMAD technique is that it can yield pure metal colloids without any byproducts of metal salt reduction, also it can provide wide industrial application by scaling up the process, guarantee the products in large amounts and with reproducible quality.

1.3 Digestive ripening process

As described above, gold nanoparticles can be gained either by bottom-up or top-down strategy, and those as prepared gold nanoparticles normally have a wide range of size distributions. In order to get monodisperse systems with narrowed size distribution and uniform shape, some post preparative process was needed. The well-known method is Ostwald ripening, which is a spontaneous process where smaller particles will disappear and form bigger particles. Unlike Ostwald ripening, digestive ripening is a process wherein a metal colloidal suspension is heated to near the boiling point of the solvent in the presence of excess capping ligands. During this process, bigger particles will be broken down and smaller ones will grow in size, and the system finally reaches a thermodynamic equilibrium. This process, used in conjuction with SMAD was first conducted in our laboratory,[22] and has been successfully employed to gain monodisperse gold, silver, copper, magnesium, and palladium colloidal system.[29-30, 39-40] It is a very simple but efficient way to convert the a polydisperse system into a monodisperse one.

1.4 Characterization techniques

In this research, the gold nanoparticles were characterized by means of Ultraviolet-Visible-Near Infra Red (UV-Vis-NIR) spectra and Transmission electron microscopy (TEM). The UV-Vis-NIR spectra were collected on a fiber optic CCD array UV-Vis spectrophotometer of Spectral Instruments, Inc. Both size and concentration of gold nanoparticles can be determined directly from UV-Vis spectra.

TEM is the most common characterization technique for investigation of the morphology of small particles. TEM was performed with a Philips CM 100 electron microscope operating at 100 kV. The samples were prepared by putting a 3 μL drop from the gold colloids onto a carbon-coated copper grid. The grid, placed above the hot plate, was allowed to dry for 15 minutes and left undisturbed at ambient conditions.

1.5 Surface plasmon resonance

Metal nanoparticles, like gold and silver, possess a plasmonic band in the visible region of the electromagnetic spectrum. Thus, spherical gold nanoparticles have a characteristic red color, while silver spheres are yellow. The d-electrons in these metals are free to travel through the material and the mean free path is about 50 nm. Therefore, in metal nanoparticles that are smaller than this means there is no free path and no scattering of light is observed, as in the case of bulky, larger particles. Thus, the interactions of light in resonance with the surface free electrons of metal nanoparticles create oscillations. As a result of this optical effect, a new type of resonance called plasmon or surface plasmon resonance (SPR) localized between the metal nanoparticles and the surrounding dielectric medium produces an enhanced electromagnetic field at the interface and experimentally these resonances can be monitored by absorption spectroscopy. The wavelength of the absorption peak maximum is found to depend on the shape, size and dielectric constant of the surrounding environment. In fact, the capping material or stabilizing ligands does influence the shift of the surface plasmon resonance. For example, thiol stabilized gold nanoparticles will give a surface plasmon resonance at 530 nm, whereas amine stabilized gold nanoparticles exhibit SPR at 540 nm. If the particle size is smaller than the wavelength of the absorption light, the shift in SPR will be in a narrow range. In the case of larger plasmonic metal nanoparticles, they exhibit a red shift.

1.6 Aims of the thesis

The aims of this thesis include the study of gold nanoparticles capped by different amines by two different methods, inverse micelle method and SMAD method. The goal is to understand the behavior and morphology of the amine capped gold colloids using these two methods. These approaches allow us to investigate the different effects of the capping ligand on gold nanoparticles, as well as the comparison between different synthesis methods.

Chapter 2. Gold-Aromatic Amine: A study of Solvated Metal Atom Dispersion method (SMAD), Digestive Ripening, Effect of the Condensing Solvent, and Ligand Concentration

2.1 Methods and materials

2.1.1 Chemicals

Gold, Aniline (98%), and Phenethylamine (98%) were obtained from Sigma-Aldrich and used without further purification. Toluene (99.9%), Ethanol (99%), and Butanone (99%) were purchased from Fisher Scientific. Toluene was dried over sodium and butanone was dried over K_2CO_3, and those solvents were distilled and degassed four times by Freeze-pump-thaw procedure prior to use.

2.2.2 Preparation Procedures

2.2.2.1 Preparation of the condensing solvents

During the SMAD procedure, the distilled and degassed toluene and butanone were used as the condensing solvents. They were degassed by the Freeze-pump-thaw procedure, during which the solvent was placed in a Schlenk tube and first flash-frozen by using liquid nitrogen (77K), then a vacuum was applied, and the tube was sealed. Next, using a warm water bath to thaw the solvent, bubbles of gas formed and escaped. This procedure was repeated four times until the pressure inside of the tube remained constant. While we operated this procedure, we found that the temperature of the liquid nitrogen was so low that occasionally the Schlenk tube would break during thawing. So in order to avoid this problem, we dipped the Schlenk tube into a Dewar full of ethanol, then poured liquid nitrogen to freeze ethanol because the melting point of ethanol is lower than the solvents. As the temperature goes down to freeze ethanol, it is low enough to make toluene and butanone frozen. This procedure proved to be a better way to save the Schlenk tubes.

2.2.2.2 Preparation of the gold-aromatic amine (aniline) as prepared colloids (SMAD method)

The tungsten crucible coated with alumina was assembled inside the SMAD reactor connecting to the two water cooled copper electrodes. Then the vacuum was applied to pump down

the whole reactor until the pressure reached 4×10^{-3} torr. The crucible was heated to red hot for about half an hour, then the reactor was cooled down naturally under vacuum overnight, to ensure no contamination. Then the reactor was filled with air and opened, 30 mg (1.5×10^{-4} mole) gold was measured and placed in the crucible and 0.417 mL (4.5×10^{-3}mole) capping ligand aniline was placed at the bottom of the reactor together with a stirring bar. The metal to ligand molar ratio was 1:30, based on previous experiments.[40] Outside of the reactor, a liquid N_2 Dewar was placed to guarantee the temperature of the wall of the reactor was maintained at 77K. The Schlenk tube, which contained the distilled and degassed toluene or butanone solvent, was connected to the SMAD reactor under the vacuum line. When the vacuum reached to 4×10^{-3} torr again, the Schlenk tube was opened to the vacuum line, and then the solvent began to be evaporated and condensed on the wall of the SMAD reactor and then formed a uniform solvent matrix. After 30 mL of the solvent was frozen, the Schlenk tube was closed a little bit, to let the condensing speed slow down; meanwhile, the metal was heated gradually using water cooled electrodes until reaching the temperature when the gold began to evaporate. The vaporized metal and the solvent vapor were co-condensed on the wall of the reactor, and this co-condensing restricts vaporized atoms from aggregation. During this time, the liquid nitrogen Dewar was kept full outside the reactor and the evaporation speed was controlled to make sure the solvent vapor condensed on the wall. The pressure of the whole process was maintained at 4×10^{-3} torr and the temperature required for the metal vaporization was about 900℃. As the reaction processed, the matrix became deep purple. At the end of the reaction, the liquid nitrogen Dewar was removed and the matrix was allowed to melt down to the bottom of the reactor stirred with aniline agitated for about an hour under argon atmosphere. Then the as-prepared gold colloid was prepared and siphoned to another Schlenk tube under argon.

During this research, appropriate cleanliness and safety procedures were carefully followed. All of the glasswares including the SMAD reactor, Schlenk tube, shower head, bridge head as well as round bottom flasks were rigorously washed before starting this procedure. They were first washed by aqua regia, and then put in the base bath overnight and later stayed in the acid bath another day and finally washed with copious amounts of water. Goggles must be worn to protect eyes while working with a vacuum line. Also, acids and bases used for cleaning can cause severe burns, so proper acid proof gloves and clothing protection are very necessary.

2.2.3 Digestive Ripening Process

2.5 mL gold-aniline as prepared colloids were dispersed in 10 mL solvent for the digestive ripening process, and the process was carried out in three different gold colloid systems (gold-aniline-toluene, gold-aniline-butanone, gold-aniline). They were under reflux at the boiling point of the solvent for 2 h.

2.2.4 Gold-aniline colloids synthesized in Butanone system

This is a single-solvent system. In this system, butanone was used as the single solvent which served as co-condensing solvent, as well as digestive ripening solvent and the digestive ripening process was carried out at the boiling point (80℃) of butanone.

2.2.5 Gold-aniline colloids synthesized in Toluene system

Similar to the butanone system, in the toluene system the toluene was used as co-condensing solvent as well as digestive ripening solvent and the digestive ripening was carried out in toluene at the boiling point (110℃) of toluene.

2.2.6 Gold colloids synthesized in pure aniline

This procedure was conducted in a two-solvent system. Butanone was used as the co-condensing solvent for the evaporated gold metal atom separation, while the digestive ripening process was carried out in pure aniline. After siphoning gold-aniline as prepared colloids into a Schlenk tube, butanone was removed under vacuum leaving gold-aniline colloids, which was then digestively ripened in pure aniline at the boiling point (185℃) of aniline.

2.2 Characterization

Analyses of the particles were carried out before and after the digestive ripening process. UV-Vis absorption spectra were obtained on a fiber optic, assisted by a DH-2000 UV-Vis optical spectrophotometer instrument (Ocean Optics Inc). Transmission electron microscopy (TEM) studies were performed on a Philips CM100 operating at 100kv. The TEM sample was prepared by placing a drop of gold colloid on a carbon coated grid and allowed to dry above the hot plate. The size distribution was calculated based on at least 200 particles. The snap shots were taken by iPhone 4.

2.3 Results and Discussion

Since 1986 when the SMAD approach for producing nanoparticles was first reported by Klabunde and coworkers[27] for the synthesis of gold colloids, lots of work has been done on the synthesis and characterization of different metal colloids in our group. Thiol-stabilized gold colloids in the acetone system have been intensively studied and are well understood. The molar ratio of gold to thiol at 1:30[26] can result in the most highly monodispersed particles. And acetone, with its nonbonding electron pairs, can serve as a reasonably good ligand for capping gold nanoparticles during the preliminary stage.[40] Based on this previous work, 1:30 gold to aniline ratio was investigated in the gold-aniline-butanone system and gold-aniline-toluene system respectively, to study the effect of the different condensing solvent (butanone or toluene) on stabilizing gold nanoparticles. Moreover, gold-aniline colloids that were digestively ripened in pure aniline were prepared to further understand the effect of the ligand concentration, as well as the competition between the condensing solvent and the capping ligand on stabilizing gold nanoparticles. The morphology and particle size distribution of these gold nanoparticles in these different systems were characterized by means of TEM and UV-Vis spectra. Representative images were selected and displayed in the figures. The results in different systems are discussed below.

2.3.1 Gold-aniline colloid in butanone system

The as prepared Au-aniline-butanone colloid has a dark purple color. TEM studies of this colloid (Figure 2.1 A) show particles with random geometrical shapes. After the digestive ripening process, the color of the colloid changed from dark purple to bright purple. TEM studies (Figure 2.1 B) show nearly spherical particles with sizes in the range of 10 to 50 nm, which indicates that the digestive ripening procedure did improve the size distribution of the gold nanoparticles. This is also confirmed by the UV/Vis absorption spectrum (Figure 2.2). The surface plasmon resonance (SPR) peak of the as prepared colloid shows a broad peak with a low absorption maximum; but as the digestive ripening process progresses, the SPR peak becomes sharper and the absorption maximum increases.

Two types of stabilization are characteristic for the as prepared gold colloid. One is steric stabilization which is obtained by the combination with butanone molecules and the other is electrostatic stabilization by acquiring electrons from the reaction vessel walls, using electrodes as

well as solvent medium. Both stabilizations took place at the same time during the warming up process, which took at least one hour to ensure good stabilization. The digestive ripening process turned out to be the key step to get monodisperse aniline capped gold colloid. Heating the as prepared colloid under reflux resulted in a narrowing of the particle size distribution.

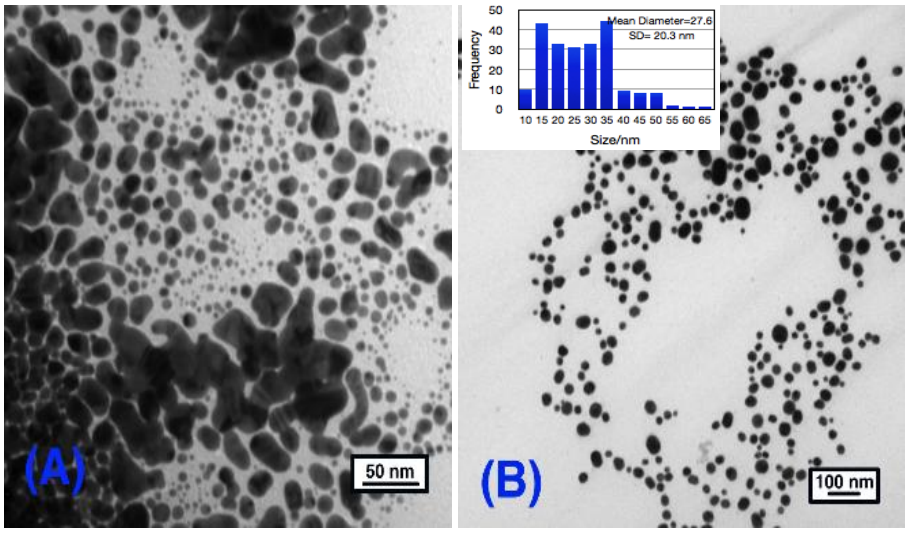

Figure 2.1 TEM images of (A) As prepared Au-aniline colloid in butanone, (B) Au-aniline colloid after digestive ripening 2 h in butanone. The particle size distribution of the digestive ripened colloid is given in the inset of (B)

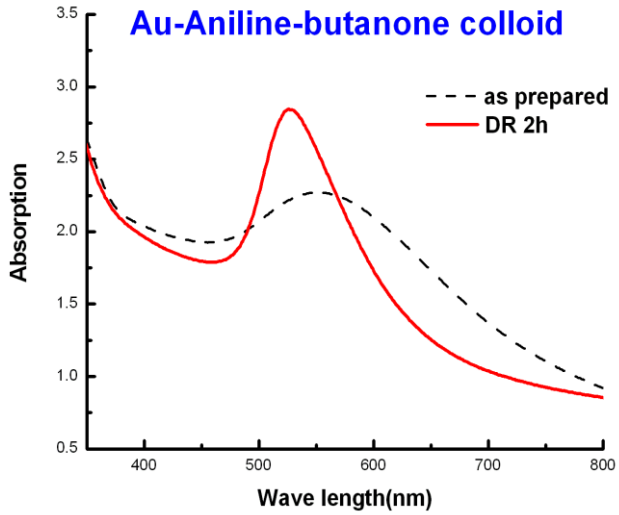

Figure 2.2 UV-visible spectrum of Au-aniline in butanone before and after digestive ripening, and the digestive ripening process kept going for 2 h

2.3.2 Gold-aniline colloid in toluene system

In the gold-aniline-toluene system, gold nanoparticles precipitated during the warming up process, and after digestive ripening, big dark clusters formed at the bottom of the flask and the supernatant was light pink. Figure 2.3 shows snap shots of Au-aniline colloids in both butanone and toluene digestive ripened after 7 days. As we can see, in the butanone, the gold colloid was yellow brown, and some gold particles precipitated. While in the Au-aniline-toluene system, the supernatant became nearly clear, almost all the particles precipitated to the bottom. The UV/Vis absorption spectrums (Figure 2.4) of the gold colloid before and after digestive ripening confirmed there was no significant change of the size distribution after digestive ripening. They are characterized by a broad plasmon absorption band with no definite maximum.

The results indicate that toluene is not a good condensing solvent, compared with butanone for the gold nanoparticles, and the digestive ripening process did not work as well in toluene. One possible explanation for the different stability of the two gold colloid systems is as follows: butanone is a polar solvent and with its nonbonding electron pairs it can act as a good ligand for gold nanoparticles at the preliminary stage. While the polarity of toluene is less, it is harder for

toluene to bind with gold atoms, so gold atoms aggregated together and big clusters formed. Once the big gold clusters formed, it's even harder for gold nanoparticles to undergo the digestive ripening process in the presence of aniline.

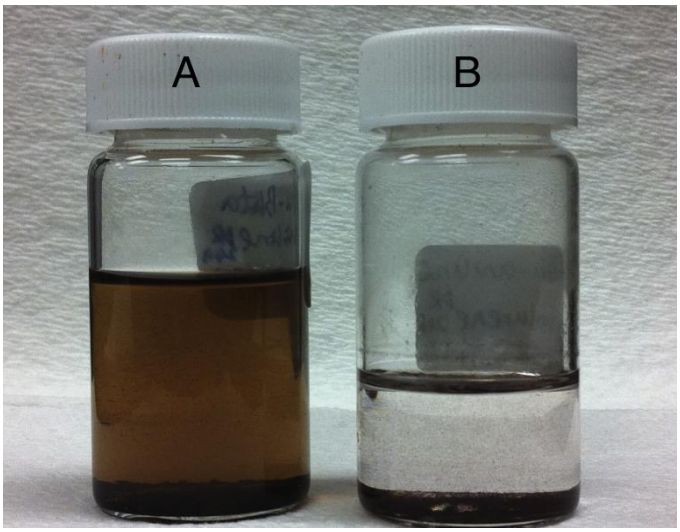

Figure 2.3 Snap shots of (A) Au-aniline colloids in butanone 7 days after digestive ripening and (B) Au-aniline colloids in toluene 7 days after digestive ripening

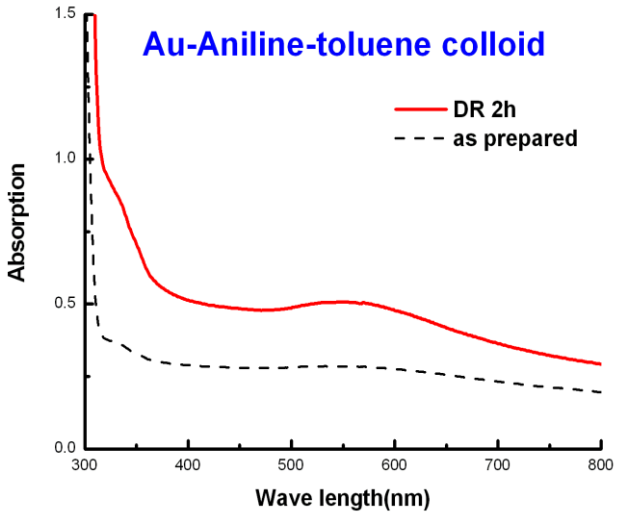

Figure 2.4 UV-Vis spectrum of Au-aniline colloids before and after digestive ripening 2 h in toluene

2.3.3 Gold-pure aniline colloids

In gold-pure aniline system, the gold colloids were under reflux in pure aniline. TEM studies (Figure 2.5 B) show that the average particle size is 4.6 ± 0.9 nm, compared with the gold-aniline in butanone system, in which the mean particle size is 28 ± 20 nm, so both the particle sizes and size distribution are much smaller. Figure 2.5 (A) shows the TEM of the same gold-pure aniline colloids after 7 days. As we can see the particles grew and aggregated to bigger ones, with mean particle size of 7.1 ± 5.3 nm. Figure 2.6 (A) shows the snap shot of Au-pure aniline colloids after 2 h digestive ripening process. The color of the gold colloid was brownish yellow, and colloid was uniform and quite stable. When kept in process for a longer time, the colloid became darker but still homogenous without any precipitates. Figure 2.6 (B) shows the digestively ripened gold-pure aniline colloid after one week.

From the results above, we could draw a conclusion that aniline does play a significant part as a capping ligand in stabilizing the gold colloid, and as the concentration of the aniline goes higher the gold colloid is more stable and the particle sizes, as well as the size distribution, become smaller. The color of the colloid became darker when kept for a longer time, probably due to the gold particles rearranging, but particle sizes are still quite small since there were no precipitates formed in this system.

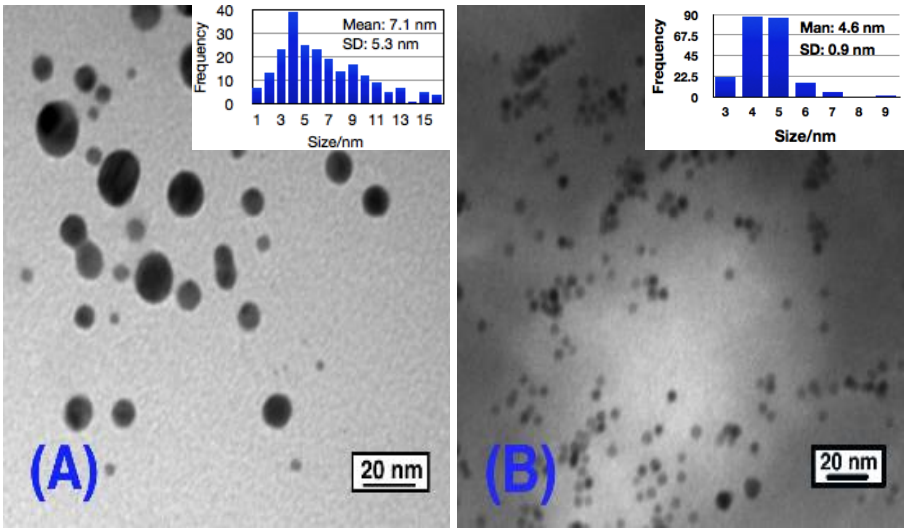

Figure 2.5 TEM images of (A) Au-pure aniline colloids after 7 days (B) Au-pure aniline colloids after digestive ripening. The particle size distributions of the Au-aniline colloid are given in the inset of (A) and (B), the mean diameter of the particle size is 7.1±5.3 nm, 4.6± 0.9 nm respectively. They were calculated by Image Pro 7.0 software based on more than 200 particles

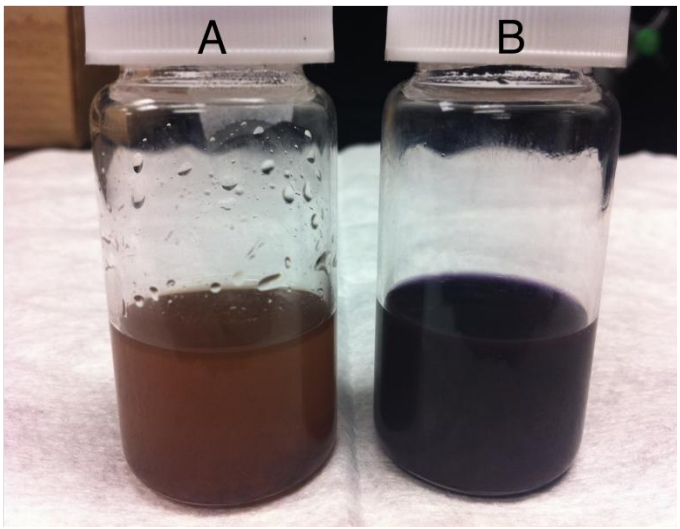

Figure 2.6 Snap shots of (A) Au-pure aniline colloids after digestive ripening process 2 h and (B) the Au-pure aniline colloids that was kept for 7 days

2.3.4 Gold-phenethylamine colloids

The gold-phenethylamine colloids were synthesized by the inverse micelle method, which will be discussed in detail in the following chapter. The digestive ripening process was carried out in butanone solution. Phenethylamine is a commonly used aromatic amine, which has similar structure as aniline. When it was used as a capping ligand in gold colloids, some interesting results were revealed. Figure 2.7 shows the TEM and UV-Vis spectra results of it. As can be clearly seen, the as prepared gold-phenethylamine (Fig.2.7 A) particles arranged nicely and tended to form a 2D monolayer. As digestive ripening progressed, the particles began to aggregate together (Fig. 2.7 B), and after 3 h almost all of the particles settled down and aggregated together, as shown in Figure.2.7(C). The UV-Vis spectra also confirm this, as it shows in Figure 2.8. After digestive ripening 2 h, the plasmon band became sharp and narrowed, indicating that the digestive ripening works during the first 2 h, when polydispersed colloids are transformed into monodispersed one. However, after 3 h, all of the particles aggregated and precipitated, as confirmed by UV-Vis spectra showing a broad band with no definite peak.

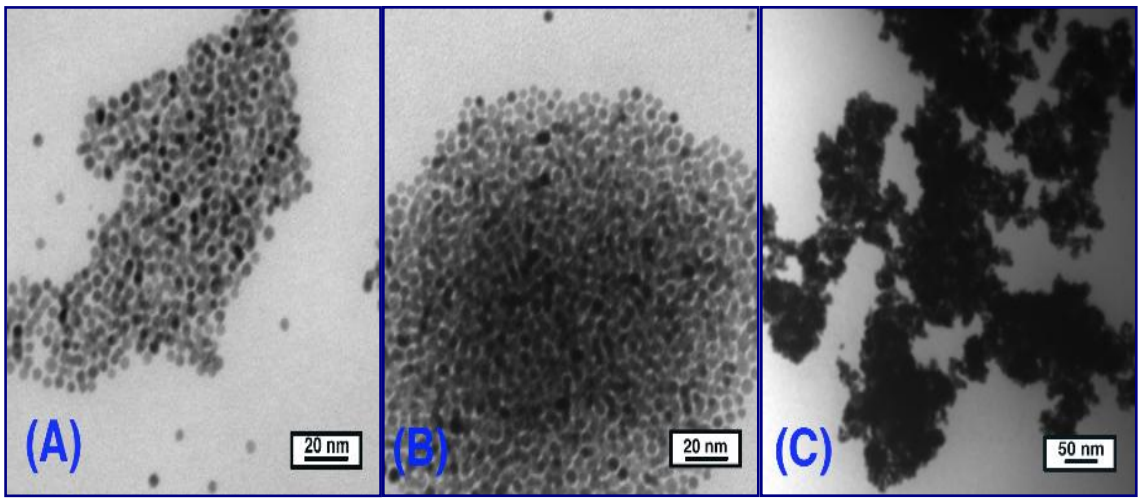

Figure 2.7 TEM images of (A) As prepared Au-phenethylamine colloids in butanone, (B) Au-phenethylamine colloids after 2 h digestive ripening in butanone, and (C) Au-phenethylamine after 3 h digestive ripening

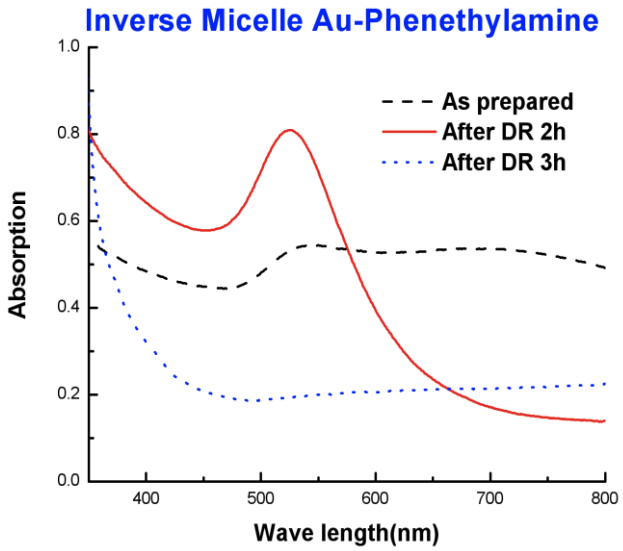

Figure 2.8 UV-visible spectrum of Au-phenethylamine colloids before and after digestive ripening

2.4 Conclusion

Aniline capped gold colloids were successfully synthesized in three different systems by the SMAD method. Butanone turned out to be a better choice for the condensing solvent as a preliminary capping ligand compared with toluene. Digestive ripening took place and greatly improved the size distribution of the gold-aniline-butanone system. The gold-aniline colloid in pure aniline system yields much smaller and more stable gold nanoparticles, which indicates that ligand concentration efficiently affects the particle sizes.

Phenethylamine capped gold colloids also synthesized by the SMAD method, butanone was used as the condensing solvent. The TEM and UV-Vis spectra results indicate that as the digestive ripening progressed, the nicely arranged as-prepared phenethylamine capped gold particles began to aggregate together, and after 3 h almost all of the particles settled down.

Chapter 3. Gold-Alkyl Amine colloids: SMAD method and Inverse Micelle method, a study of Digestive Ripening, Stabilizing Ligands and Particle Size Distribution

3.1 Methods and Materials

3.1.1 Chemicals

Didodecyldimethylammonium bromide (DDAB) was purchased from Fluka and used as received. Sodium borohydride, gold chloride (99.99%), Bulk Gold, butylamine (98%), octylamine (98%), dodecylamine (98%), hexadecylamine (98%), and octadecylamine (98%) were purchased from Sigma-Aldrich and used without further purification. Deionized distilled water was obtained from a Barnstead nanopure system. Toluene (99.9%), ethanol (99%) and Butanone (99%) were purchased from Fischer Scientific. The toluene and butanone were distilled, and degassed four times by the Freeze-pump-thaw procedure before use in SMAD experiments.

3.1.2 Preparation of Au-phenethylamine, Au-butylamine, Au-octylamine, Au-dodecylamine, Au-hexadecylamine, Au-octadecylamine as prepared colloids by inverse micelle method. Specific methods for gold nanoparticles

3.1.2.1 Preparation of the as prepared gold colloid

The gold-amine as prepared colloid was prepared at room temperature using a DDAB/water/toluene inverse micelle system. Lots of work [41] has been done to get nanoparticles with a fairly narrow size distribution by carefully controlling the amount of water, surfactant, and the rate of reaction, as well as the reaction temperature. In order to study the effect of digestive ripening on the particle size distribution, a smaller amount of DDAB surfactant was used to create a polydisperse colloid.[26] A typical synthesis is as follows. A 0.025M micelle solution was formed by adding 156 mg of DDAB (3.8×10^{-4} mole) in 15 mL toluene, and the toluene was degassed by bubbling with argon gas 2 h prior to use. Then 51 mg gold chloride (1.5×10^{-4} mole) was measured and dissolved in the micelle solution and sonicated for 15 min, to obtain a clear reddish brown colored solution. Meanwhile, a 9.4M $NaBH_4$ solution was formed by adding 0.178 g $NaBH_4$ (4.7×10^{-3} mole) to 0.5 mL deionized water, 54 μL of that (5×10^{-5}mole) was added dropwise to the

gold chloride micelle solution. The color of the solution changed to dark brown within one minute. Thus, the as prepared gold colloid was obtained after vigorously stirring for 30 min at room temperature. Then 5 mL of the as prepared gold colloid was transferred to a separate 30 mL vial to which different amine was added at the bottom, together with a stirring bar. To keep the molar ratio of Au/amine at 1:30, phenethylamine (0.8 mL), butylamine (0.8 mL), octylamine (0.8 mL), dodecylamine (0.308 g), hexadecylamine (0.401 g), and octadecylamine (0.448 g) were used during this experiment. After stirring for 1 min within each vial, the color of the colloid turned to purple. Similar to Dodecanethiol, these amines also have an affinity to the gold surface[42] which results in a change of the interaction strength between the particles. The purple color was caused by the aggregation of the gold particles.[43]

3.1.2.2 Isolation of the dried gold particles

The amine capped gold nanoparticles were then separated from the DDAB, excess amine, and the reaction by-product by precipitating with 15 mL of ethanol. After letting the vial stand undisturbed overnight, the particles which settled down to the bottom were isolated from the supernatant by decanting and vacuum drying.

3.1.2.3 Digestive Ripening

The dried precipitates were redissolved into 5 mL toluene and transferred to a 50 mL round bottom flask, and the same amount of amine was added to the flask for digestive ripening process. Reflux of the each mixture for 2 h under an argon atmosphere led to the formation of monodisperse colloids. Figure 3.1 shows the inverse micelle procedure and digestive ripening.

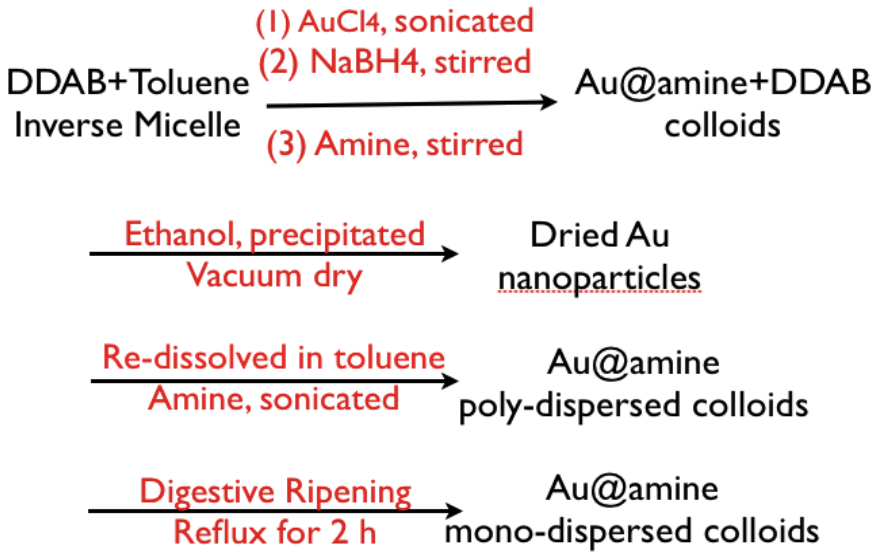

Figure 3.1 Schematic representation of the synthesis of gold colloid by inverse micelle method and digestive ripening process

3.1.3 Preparation of Au-butylamine, Au-octylamine, Au-dodecylamine, Au-hexadecylamine, Au-octadecylamine as prepared colloids by SMAD method

3.1.3.1 Preparation of the as prepared gold colloid

The SMAD technique allows synthesis of pure gold colloids on a large scale. Chapter 2 provides a detailed description of the Au nanoparticle preparation by the SMAD procedure. The process was carried out under dynamic vacuum (4×10^{-3} Torr) in a settled reactor covered by liquid nitrogen Dewar. Bulk Au (150 mg) was heated by the electrodes in the crucible and then evaporated and co-deposited with butanone vapors (120 mL) on the walls of the reactor. At the end of this procedure, the liquid nitrogen Dewar was removed and the dark purple Au-butanone matrix was allowed to melt down. After stirring for about 1 h, the Au-butanone solution was siphoned into five vessels, which each contained a different amine (phenethylamine (0.6 mL), butylamine (0.6 mL), octylamine (0.6 mL), dodecylamine (0.224 g), hexadecylamine (0.292 g), and octadecylamine (0.325 g)) at the bottom. Each one was pumped down to remove butanone under vacuum. Then agitation was commenced for each vessel for about 2 h under argon atmosphere. Then the Au-amine

as prepared colloid was diluted to 80 mL with toluene for the preparation of the digestive ripening process.

3.1.3.2 Digestive Ripening

The gold-amine-butanone as prepared colloid was then refluxed at the boiling point of toluene for 2 h under argon atmosphere. The final colloidal solution contains high quality Au nanoparticles stabilized by a different amine. Figure 3.2 shows the synthesis of gold colloid procedure by SMAD method and digestive ripening process.

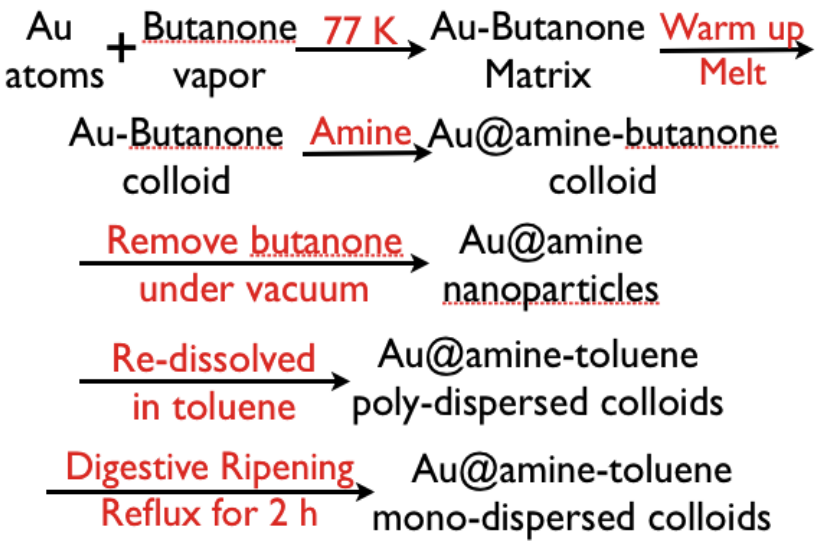

Figure 3.2 Schematic representation of the synthesis of gold colloid by SMAD method and digestive ripening process

3.3 Characterization

3.3.1 UV-Vis Spectroscopy

UV-Vis spectra were taken on a Spectral Instruments 400 series spectrophotometer, and toluene solvent was used.

3.3.2 Transmission Electron Microscopy

TEM images were taken with a Philips EM100 microscope operating at 100kV. The particle size distributions were determined from a sample of a minimum of 200 particles. The diameter of these particles was measured by using software. Every distance was accurate to the fifth decimal place and the mean particle size and stand distribution were calculated based on these original data.

3.4 Results and Discussion

3.4.1 Gold-amine by Inverse Micelle method: The effect of Alkyl chain length

A series of alkylthiols were used as capping ligands for gold colloid in our previous work.[44] It is very encouraging to find out that the digestive ripening process significantly reduced the average particle size and polydispersity, and formed separate particles with longer chain length (C16) thiols and aggregatde into 3D superlattices with short chain length (C8 and C10) thiols. Those superlattices have similar solubility behaviors to those of normal molecular solids.[22] Inspired by that finding, our group recently focused on using different amines as the capping ligand, by the same synthesis method, to investigate the particle behavior of the gold-amine colloids. The results are discussed in detail below.

Different gold-amine colloids were synthesized by the inverse micelle method. The highly poly-dispersed gold colloids capped by DDAB are depicted in Figure 3.3. The addition of the different amine leads to many changes. Big polyhedral particles transformed into much more uniform particles, with sizes ranging from 8 to 22 nm. The morphologies and particle sizes of those as prepared gold colloids are very different due to the different capping ligands; they all easily settled down with different color, changing from dark blue to dark purple as the chain length of the ligands increases. The following procedure is digestive ripening, during which all gold colloids were reddish purple homogenous solution under reflux temperature of toluene, while visible changes appeared when they cooled down to room temperature. Au-butylamine (Au-C_4N) colloids settled down quickly at the bottom, forming dark blue precipitates with almost clear supernatant. The dark purple particles of Au-octylamine (Au-C_8N) colloid were also easy to precipitate, leaving a pink supernatant. The colloids of Au-dodecylamine (Au-$C_{12}N$), Au-hexadecylamine (Au-$C_{16}N$)

and Au-octadecylamine (Au-$C_{18}N$) are very similar to each other. After cooled down, the color changed from reddish purple to purple, some purple precipitates formed and the supernatant remained purple color. The morphologies and particle sizes of the gold colloids were characterized by TEM before and after digestive ripening. The digestive ripening procedure greatly improved the particle size distribution. As can be clearly seen from the TEM images (Figure 3.4, 3.6, 3.8, 3.10 and 3.12), a polydisperse colloid containing particles with sizes ranging widely transformed into an almost monodisperse colloid with narrow particle sizes distribution. The mean diameters of the Au-C_4N, Au-C_8N, Au-$C_{12}N$, Au-$C_{16}N$ and Au-$C_{18}N$ colloids were 17.2 ± 4.5, 16.9 ± 2.8, 8.8 ± 1.1, 12.1 ± 2.5 and 10.4 ± 1.6 nm respectively. As for the morphology of these gold colloids, except for Au-C_4N nanoparticles, which easily aggregated together and formed 3D superlattices, the others have a tendency to organize into 2D layers and the shape of the particles is more polyhedral rather than spherical after digestive ripening.

The UV/Vis absorption spectrum results (Figure 3.5, 3.7, 3.9, 3.11 and 3.13) taken before and after digestive ripening of each gold-amine colloid are in complete agreement with the TEM observations. The optical spectra of the as prepared colloids of Au-C_4N, Au-C_8N and Au-$C_{12}N$ show similar broad plasmon absorption bands with no definite maximum. Au-$C_{16}N$ and Au-$C_{18}N$ as prepared colloid reveals a broad peak with a peak maximum around 570 nm. As for the digestive ripened gold colloids, all show a sharp and narrow peak around 530 nm, indicating a dramatic narrowing of the particle size and distribution, except for Au-C_4N, which has a broad plasmon with a large tail above 700 nm.

It has been fully discussed now that the optical properties of gold colloids are mainly decided by the particle aggregation, particle sizes and distribution as well as interparticle separation.[45] Thus, the large tail observed for Au-C_4N indicates that the particles are aggregating together which agrees with the TEM images (Figure 3.4). The red shift of the colloid in UV-Vis spectra was caused by the stronger electromagnetic coupling between the particles, which happens when the superlattices are bigger, and the ligand chain length separating the particles is smaller.

The observations obtained above suggest that the chain length of amine has a great impact on the particle size variation and interparticle separation. Simple explanations like " lengthier ligands stabilize larger particles"[47] do not explain this phenomenon because as we can clearly see from the TEM images that $C_{12}N$ leads to the smallest particle sizes and narrowest size distribution

(8.8 ± 1.1 nm), smaller than the longer ligands which are $C_{16}N$ (12.1 ± 2.5 nm) and $C_{18}N$ (10.4 ± 1.6 nm). Many proposals have been reported on the stabilization of nanoparticles suggesting that control may be due to thermodynamics other than the kinetics of nucleation and crystal growth.[48] They discussed that the nanoparticle size resulted from a combination of the ligand-gold binding energy and the surface free energy of the particles to reach the minimum energy of the whole system. The ligand-gold binding energy favors smaller particles with larger surface areas, while the surface free energy favors larger particles with smaller surface curvature. Therefore, these two effects oppose each other and lead to a minimum energy with a thermodynamically favored size for each gold-amine colloid system.

As for the interparticle separation, it seems that the bigger particles are more likely to aggregate into 3D superlattices, and the smaller ones are more likely to form separate particles. One possible explanation for this tendency can be rationalized from the attraction energy between the particles. To understand qualitatively the interparticle features, we have calculated the van der Waals attraction potential between the particle cores, utilizing the equation shown below:[49]

$$V(D) = \frac{-A}{12}\left[\frac{R}{D\left[1+\frac{D}{2(R_1+R_2)}\right]}\right] + \frac{1}{1+\frac{D}{R}+\frac{D^2}{4R_1R_2}} + 2\ln\left(D\frac{\left[1+\frac{D}{2(R_1+R_2)}\right]}{1+\frac{D}{R}+\frac{D^2}{4R_1R_2}}\right)$$

Here, A is the Hamaker constant, for gold it is 1.95 eV. R_1 and R_2 are the radii of the two spheres between which the attraction forces are to be calculated. D is the distance between the nearest surfaces of two adjacent spheres. Since the spheres are separated by the amine, we have assumed that the two alkyl chains attached to the two adjacent gold particles are fully interdigitated; that means D equals to the chain length of the amine. R is the reduced radius given by $2 R_1 R_2 / (R_1 + R_2)$; in our case $R_1=R_2=R$. The attraction potentials turn out to be -2.7 eV, -1.5 eV, -0.61 eV, -0.72 eV and -0.62 eV for Au-C_4N, Au-C_8N, Au-$C_{12}N$, Au-$C_{16}N$ and Au-$C_{18}N$, respectively. From these results, we can clearly expect Au-C_4N and Au-C_8N to favor aggregation since the attraction energies are larger than the others.

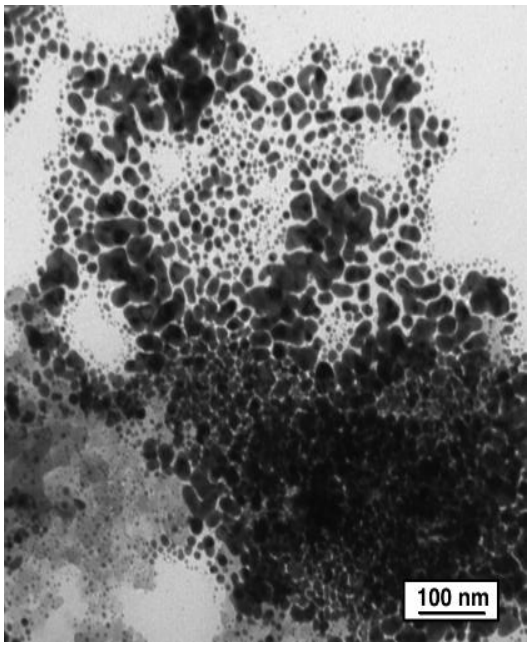

Figure 3.3 TEM images of Au-DDAB colloid in toluene by inverse micelle method

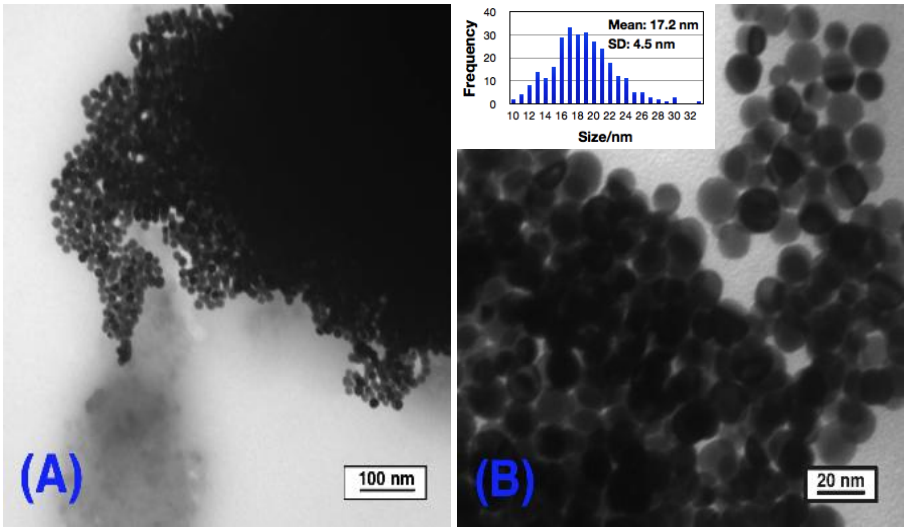

Figure 3.4 TEM images of (A) as prepared Au-butylamine colloid in toluene by inverse micelle method, (B) Au-butylamine colloid after digestive ripening 2 h in toluene

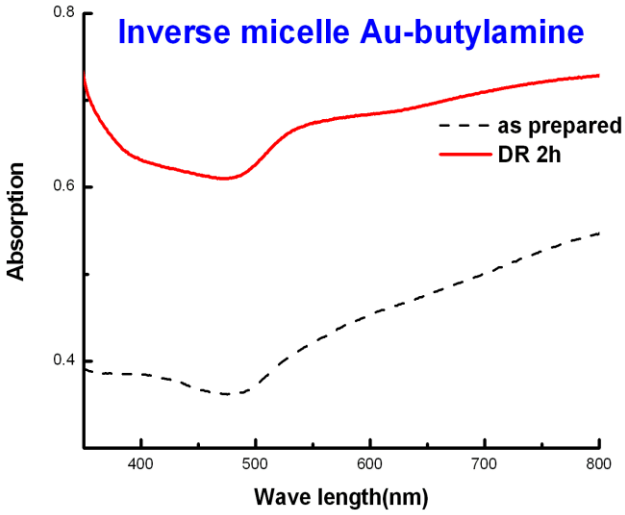

Figure 3.5 UV-Visible spectrum of Au-butylamine colloid by inverse micelle method before and after digestive ripening 2 h

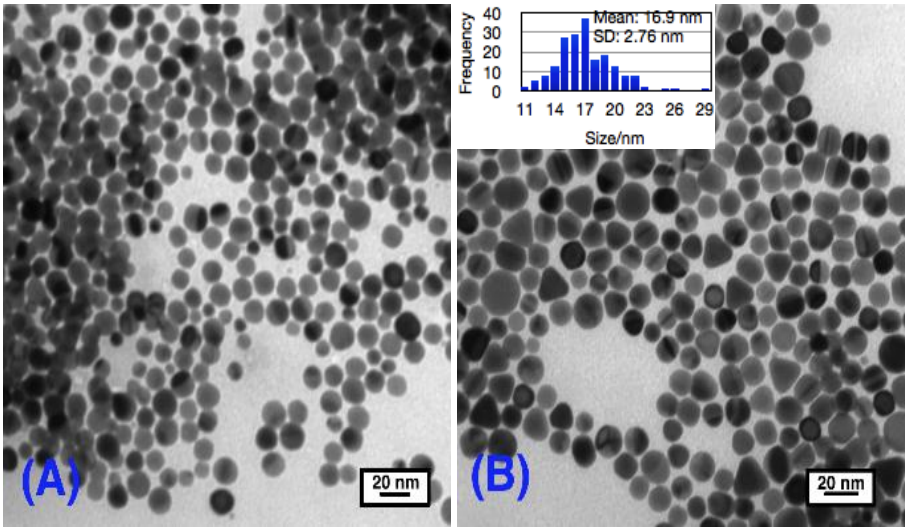

Figure 3.6 TEM images of (A) as prepared Au-octylamine colloid in toluene by inverse micelle method, and (B) Au-octylamine colloid after digestive ripening 2 h in toluene

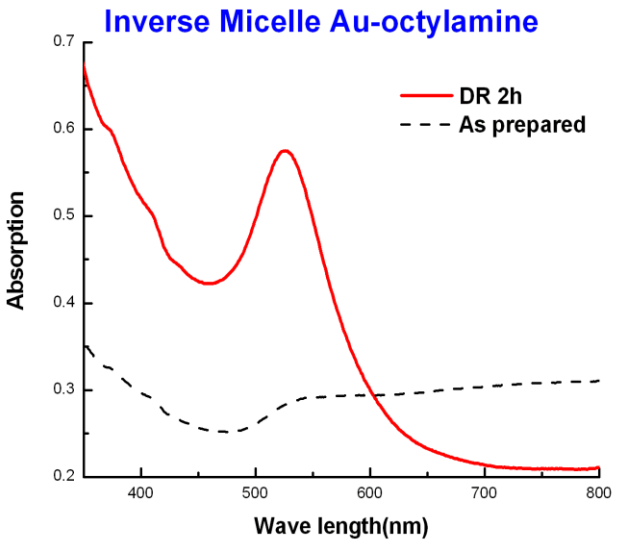

Figure 3.7 UV-Visible spectrum of Au-octylamine colloid by inverse micelle method before and after digestive ripening 2 h in toluene

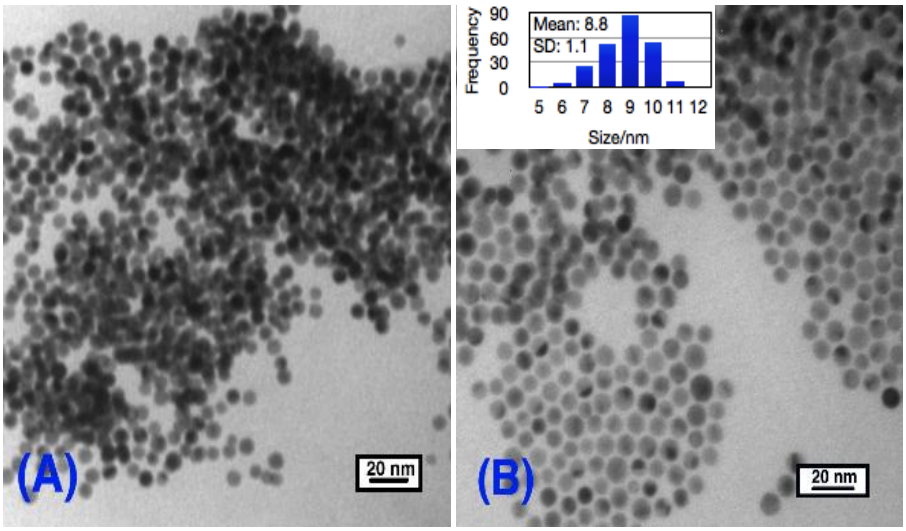

Figure 3.8 TEM images of (A) as prepared Au-dodecylamine colloid by inverse micelle method in toluene, (B) Au-dodecylamine colloid after digestive ripening 2h in toluene

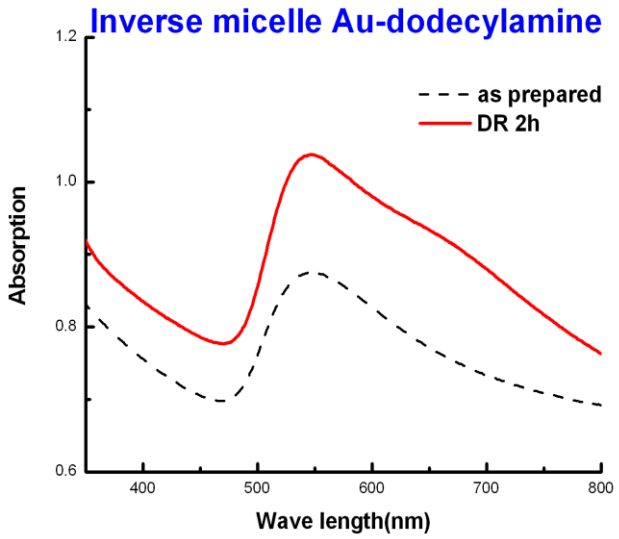

Figure 3.9 UV-Visible spectrum of Au-dodecylamine colloid by inverse micelle method before and after digestive ripening 2 h in toluene

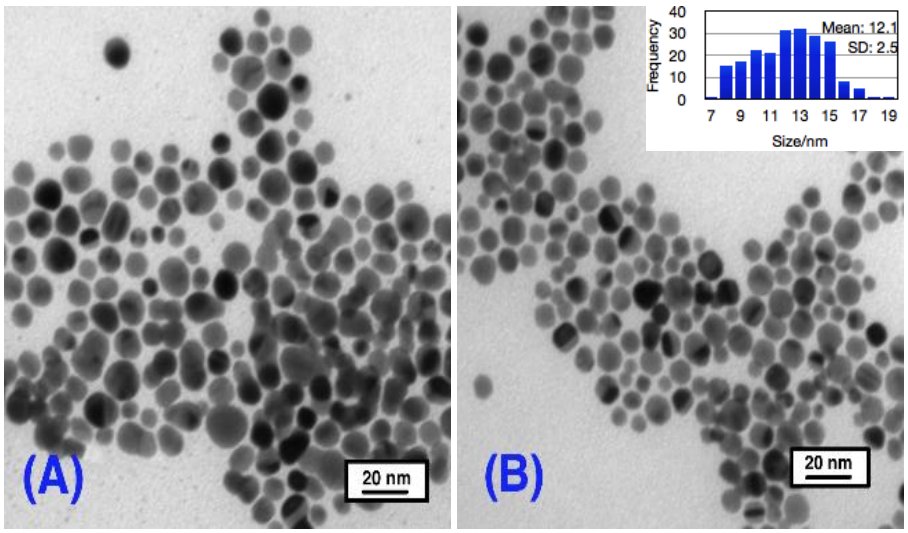

Figure 3.10 TEM images of (A) as prepared Au-hexadecylamine colloid by inverse micelle method in toluene, (B) Au-hexadecylamine colloid after digestive ripening 2 h in toluene

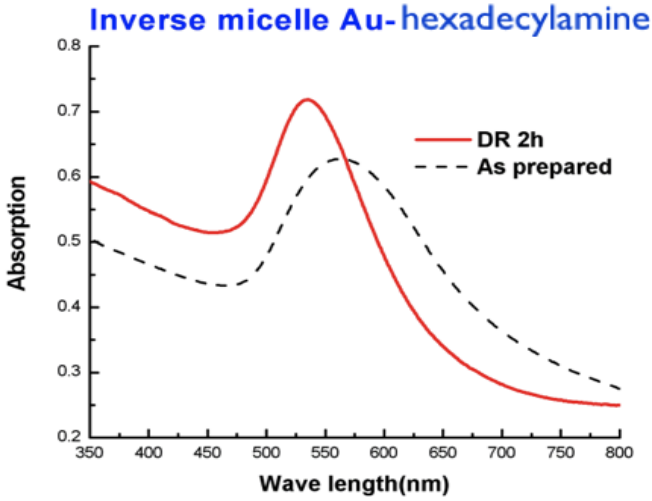

Figure 3.11 UV-Visible spectrum of Au-hexadecylamine colloid by inverse micelle method before and after digestive ripening 2 h in toluene

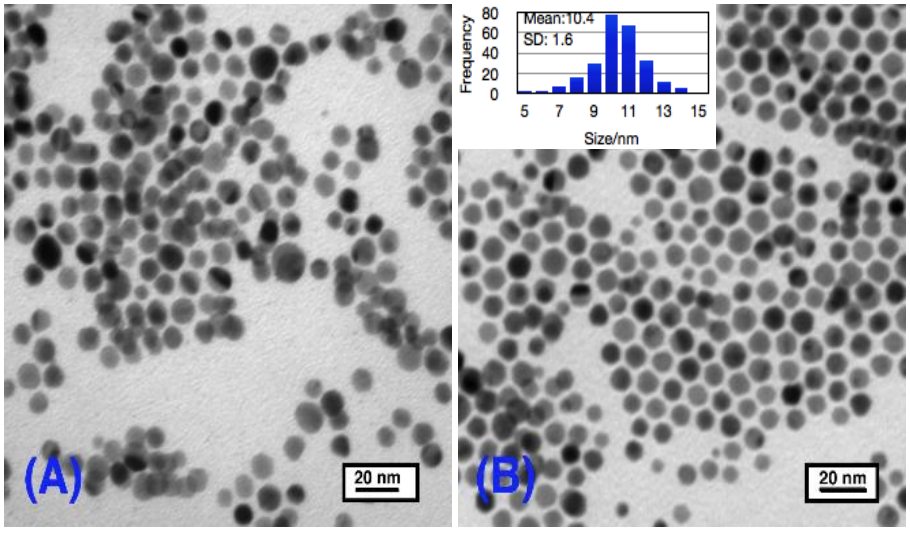

Figure 3.12 TEM images of (A) as prepared Au-octadecylamine colloid in toluene, (B) Au-octadecylamine colloid after digestive ripening 2 h in toluene

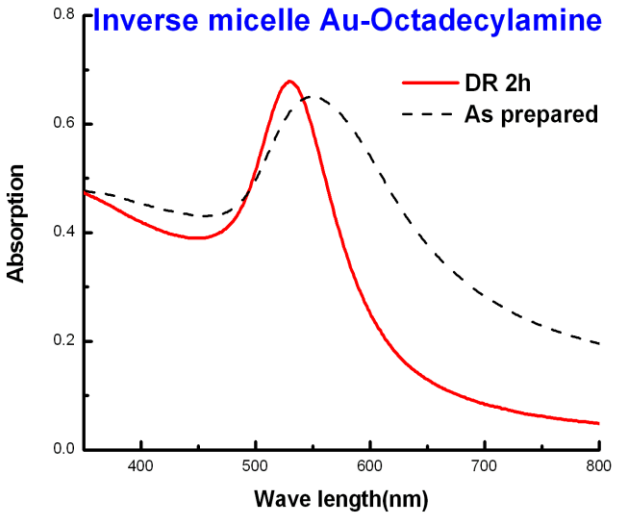

Figure 3.13 UV-Visible spectrum of Au-octadecylamine colloid before and after digestive ripening 2 h in toluene

3.4.2 Gold-amine by the SMAD method: The effect of Alkyl chain length, Comparison between Inverse Micelle and SMAD method

Gold-amine colloids that were capped by C_4N, C_8N, $C_{12}N$, $C_{16}N$ and $C_{18}N$ ligands were also synthesized by the SMAD method. The as prepared colloids which were pre-stabilized by butanone were divided into five portions along with different amine ligands. Then the solvent butanone was removed from those colloids by vacuum, and toluene was added. The colloids were re-dispersed and digestively ripened in toluene. TEM and UV-Vis were also conducted to characterize the morphologies and particle size distributions of the gold colloids before and after digestive ripening. However, it seems that there are no significant changes during the digestive ripening process. Before the digestive ripening, the color of the gold-amine colloids changed from dark blue to dark purple as the ligand length increases, and some precipitates formed at the bottom, while after being refluxed in toluene and cooled down to room temperature, the color of the each gold colloid stayed the same. The Au-C_4N and Au-C_8N colloids were settled down easily with almost colorless supernatants. Some precipitates were also formed in Au-$C_{12}N$, Au-$C_{16}N$ and Au-$C_{18}N$ colloids and the supernatant was purple color. Figure 3.14 shows the TEM images for Au-C_4N, Au-C_8N, Au-$C_{12}N$, Au-$C_{16}N$ and Au-$C_{18}N$ colloids after digestive ripening. Very interesting

results were obtained, as can be clearly seen. The morphology of these gold colloids, except for Au-$C_{12}N$, were no longer polyhedral spheres; they tended to form rod shapes, and the Au-C_4N and Au-C_8N particles aggregated together forming 3D superlattices, while the Au-$C_{16}N$ and Au-$C_{18}N$ colloids have a tendency to organize into 2D layers. As for Au-$C_{12}N$, after digestive ripening the particles were organized nicely forming 2D monolayer spherical particles with mean size 9.4 ± 1.2 nm, compared with the Au-$C_{12}N$ colloid synthesized by inverse micelle method with particles mean size 8.8 ± 1.2. The morphologies are similar, but particles sizes are bigger. The UV-Vis spectra were in total agreement with those observations. As can be seen from Figure 3.15, which shows the surface plasmon absorption of Au-C_4N, Au-C_8N, Au-$C_{12}N$, Au-$C_{16}N$ and Au-$C_{18}N$ colloids after digestive ripening, the plasmon band of both the Au-C_4N and Au-C_8N have a large tail above 700 nm, which illustrates that the particles are forming aggregates. Au-$C_{12}N$ colloids have a shoulder centered at 630nm after the 530nm peak, which reveals some particles forming 3D superlattices. As for Au-$C_{16}N$ and Au-$C_{18}N$, we can see a broad gold plasmon peak around 530nm.

The morphologies of these gold amine colloids synthesized by inverse micelle method and SMAD method are quite different. The morphologies of the inverse micelle colloids are more like polyhedral spheres, nicely arranged, while the shape of the SMAD colloids are very irregular except for Au-$C_{12}N$. The particle morphologies of the Au-$C_{12}N$ colloids by both methods are very similar, but the SMAD method yields bigger particle sizes. The differences can be explained by the different synthesis route of the two techniques. In the inverse micelle method, the nucleation and crystal growth are controlled by three factors: 1) the presence of DDAB, 2) the controlled reaction temperature, and 3) the reaction speed. While in the SMAD method, atoms aggregate and crystals grow in a more chaotic manner, since the vaporization and aggregation speed of the atoms is too fast to control. Previous work in our group has reported that particles synthesized by the inverse micelle technique preferentially assemble into face-centered cubic (fcc) structures, while the SMAD nanoparticles behave like “hard” spheres and predominantly organize into hexagonal close-packed (hcp) nanocrystal superlattices.[50] Although the digestive ripening process was carried out in both synthesis methods, it seems that it was less effective regarding core particle size adjustments when the SMAD method was used, as compared to the inverse micelle method.

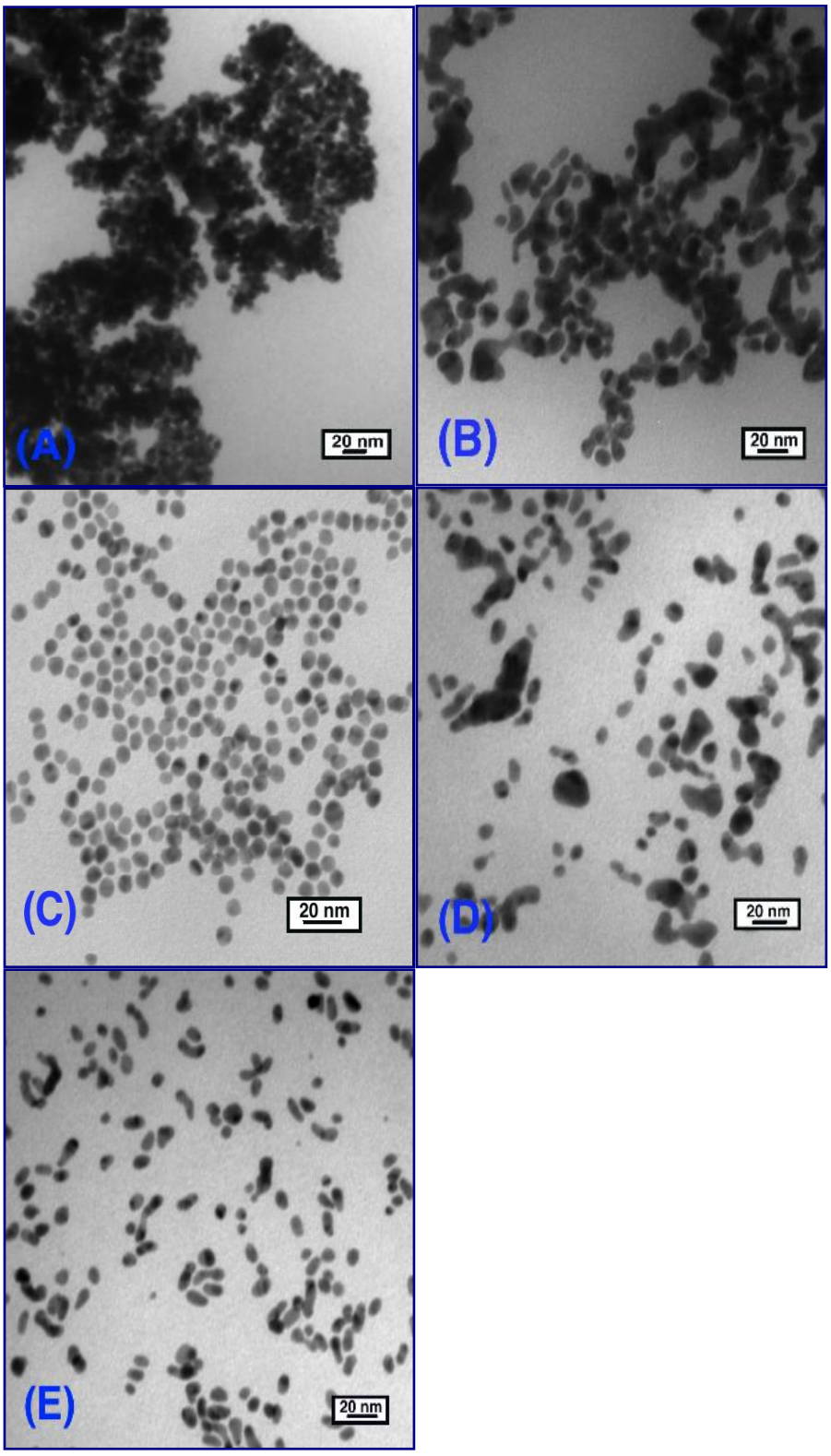

Figure 3.14 TEM images of (A) Au-C_4N, (B) Au-C_8N, (C) Au-$C_{12}N$, (D) Au-$C_{16}N$ and (E) Au-$C_{18}N$ colloids after digestive ripening in toluene

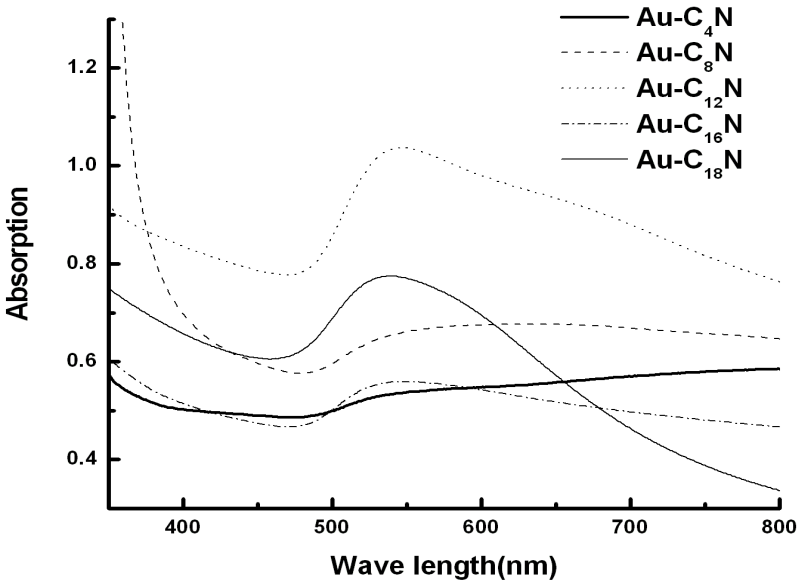

Figure 3.15 Comparison of surface plasmon resonance of these gold-amine colloids after digestive ripening in toluene

3.4.3 Comparison between alkylthiol and alkylamine as the the capping ligand for gold colloids

The properties of thiol capped gold nanoparticles have been well investigated, including their monodispersity, the fact that they are easily isolated, as well as their nature to self-assemble into superlattices. The most stable gold colloid was that using dodecanethiol ($C_{12}S$) as the capping agent. After digestive ripening, it yielded a monodispersed gold colloid with an average size of 4.7 nm by inverse micelle method.[51] In contrast, digestively ripened by dodecylamine ($C_{12}N$) leads to larger particles with an average size of 8.8 nm. Recently, the nature of the ligand-gold bonding has been reported that thiol is bound to the gold surface as a thiolate with the release the hydrogen.[52] Compared to sulfur in thiol ligands, nitrogen in amine ligands binds less strongly with the gold surface. Thus, we can conclude that less ligand-gold binding energy leads to the larger core-particle sizes, which is also in support of the proposal we discussed above that a combination of a curvature-dependent surface energy and the ligand-gold binding energy leads to the particular size of nanoparticle.

3.3 Summary

For the gold alkyl-amine colloids synthesized by the inverse micelle method, the digestive ripening process greatly changed the particle size distribution, and transformed the polydispersed colloid into a monodispersed colloid. As the chain length increases from Butylamine (C_4N) to octadecylamine ($C_{18}N$), the gold particle size decreases with more narrowed size distribution, except for Au-$C_{12}N$ colloid, which yields the smallest particle sizes and the most narrow size distribution. The bigger particles, like Au-C_4N and Au-C_8N, seem to very easily aggregate and almost all the particles settled down and formed 3D superlattices. Smaller particles, like Au-$C_{12}N$, Au-$C_{16}N$ and Au-$C_{18}N$, have a tendency to form 2D monolayers; but when kept for longer time, can still form 3D superlattices.

As to the gold colloids by SMAD method, the digestive ripening process did not take place in most of the cases; because the SMAD particles are more like "hard" sphere, it is hard for the surface process to transform the core structure of the the crystal. TEM images show that the dodecylamine capped Au colloids ($C_{12}N$) are nicely arranged to polyhedral sphere. With an average particle size of 9.4 ± 1.2 nm, the particle sizes are bigger than the Au-$C_{12}N$ colloids by inverse micelle method. The morphologies of Au colloids that are capped by C_4N, C_8N, $C_{16}N$ and $C_{18}N$ are irregular, so it's hard to determine the particle size and size distribution. Au-C_4N and Au-C_8N very easily aggregate and settled down.

Compared with the alkyl-thiol as the capping ligand for gold colloids, amine capped gold nanopartilces are bigger, which indicates that stronger ligand binding can lead to smaller particle sizes. The final particle sizes of the colloid were determined by a combination of a curvature-dependent surface energy and the ligand-gold binding energy to reach a minimum free energy of the system.

References

(1) Faraday, M. *Philos*. *Trans*.**1857,** 147, 145-181.

(2) Eustis, S.; Mostafa, A. *Chem*. *Soc*. *Rev*., **2006**, 35, 209-217.

(3) Turkevitch, J.; Stevenson, P. C.; Hillier, J. *Discuss*. *Faraday Soc*. **1951,** *11*, 55-75.

(4) (a) Giersig, M.; Mulvaney, P. *Langmuir* **1993,** *9*, 3408-3413. (b) Hasan, M.; Bethell, D.; Brust, M. *J*. *Am*. *Chem*. *Soc*. **2003,** *125*, 1132- 1133.

(5) Bethell, D.; Brust, M.; Schiffrin, D. J.; Kiely, C. *J*. *Electroanal*. *Chem*. **1996,** *409*, 137-143.

(6) Rowe, M. P.; Plass, K. E.; Kim, K.; Kurdak, C.; Zellers, E. T.; Matzger, A. J. *Chem*. *Mater.* **2004,** *16*, 3513-3517.

(7) Yee, C. K.; Jordan, R.; Ulman, A.; White, H.; King, A.; Rafailovich, M.; Sokolov, J. *Langmuir* **1999,** *15*, 3486-3491.

(8) Hostetler, M. J.; Wingate, J. E.; Zhong, C. J.; Harris, J. E.; Vachet, R. W.; Clark, M. R.; Londono, J. D.; Green, S. J.; Stokes, J. J.; Wignall, G. D.; Glish, G. L.; Porter, M. D.; Evans, N. D.; Murray, R. W. *Langmuir* **1998,** *14*, 17-30.

(9) Chen, S. H.; Kimura, K. *Langmuir* **1999,** *15*, 1075-1082.

(10) Templeton, A. C.; Chen, S. W.; Gross, S. M.; Murray, R. W. *Langmuir* **1999,** *15*, 66-76.

ller, M.; Aberle, T.; Schmidt, J.; Burchard, W. *Macromolecules* **2000,** *33*, 4791-4798.

(12) Sau, T. K.; Pal, A.; Jana, N. R.; Wang, Z. L.; Pal, T. *J*. *Nanopart*. *Res*. **2001,** *3*,257- 261.

(13) Meltzer, S.; Resch, R.; Koel, B. E.; Thompson, M. E.; Madhukar, A.; Requicha, A. A. G.; Will, P. *Langmuir* **2001,** *17*, 1713-1718.

(14) Chen, W.; Cai, W. P.; Liang, C. H.; Zhang, L. D. *Mater. Res*. *Bull*. **2001,** *36*, 335-342.

(15) Chen, W.; Cai, W.; Zhang, L.; Wang, G.; Zhang, L. *J*. *Colloid Surf*. *Sci*. **2001,** *238*, 291-295.

(16) Pol, V. G.; Gedanken, A.; Calderro-Moreno, J. *Chem*. *Mater.* **2003,** *15*, 1111-1118.

(17) (a) Henglein, A.; Meisel, D. *Langmuir* **1998,** *14*, 7392-7396. (b) Dawson, A.; Kamat, P. V. *J*. *Phys*. *Chem*. *B* **2000,** *104*, 11842-11846.

(18) Gachard, E.; Remita, H.; Khatouri, J.; Keita, B.; Nadjo, L.; Belloni, J. *New J*. *Chem*. **1998,** 1257-1265.

(19) Khomutov, G. B. *Colloids Surf*. **2002,** 243-267.

(20) (a) Nakamoto, M.; Yamamoto, M.; Fukusumi, M. *Chem*. *Commun*. **2002,** 1622- 1623. (b) Shimizu, T.; Teranishi, T.; Hasegawa, S.; Miyake, M. *J*. *Phys*. *Chem*. *B* **2003,** *107,* 2719-2724. (c) Teranishi, T.; Hasegawa, S.; Shimizu, T.; Miyake, M. *Adv*. *Mater.* **2001,** *13,* 1699-1701.

(21) Choy, K. L.**,** *Handbook of Nanostructured Materials and Nanotechnology Academic Press* ***2000*** *volume 1*.

(22) Stoeva, S.; Klabunde, K. J.; Sorensen, C. M.; Dragieva, I. *J*. *Am*. *Chem*. *Soc*. **2002,** *124,* 2305-2311.

(23) Stoeva, S. I.; Smetana, A. B.; Sorensen, C. M.; Klabunde, K. J. *J*. *Colloid Interface Sci*. **2007,** *309,* 94-98.

(24) Smetana, A. B.; Klabunde, K. J.; Sorensen, C. M. *J*. *Colloid Interface Sci*. **2005,** *284,* 521-526.

(25) Cingarapu, S.; Yang, Z.; Sorensen, C. M.; Klabunde, K. J. *Chem*. *Mater.* **2009,** *21,* 1248-1252.

(26) Lin, X. M.; Sorensen, C. M.; Klabunde, K. J. *J*. *Nanopart*. *Res*. **2000,** *2,* 157-164.

(27) Lin, S.; Franklin, M. T.; Klabunde, K. J. *Langmuir* **1986,** *2,* 259-260.

(28) Ponce, A. A.; Klabunde, K. J. *J*. *Mol*. *Catal*. *A: Chem*. **2005,** *225,* 1-6.

(29) Kalidindi, S. B.; Jagirdar, B. R. *Inorg*. *Chem*. *(Washington, DC, U*. *S.)* **2009,** *48,* 4524-4529.

(30) Naoe, K.; Petit, C.; Pileni, M. P. *The Journal of Physical Chemistry C* **2007,** *111,* 16249-16254.

(31) Hostetler, M. J.; Murray, R. W. *Curr*. *Opin*. *Colloid Interface Sci*. **1997,** *2,* 42-50.

(32) Templeton, A. C.; Wuelfing, M. P.; Murray, R. W. *Acc*. *Chem*. *Res*. **2000,** *33,* 27-36.

(33) Whetten, R. L.; Shafigullin, M. N.; Khoury, J. T.; Schaaff, T. G.; Vezmar, I.; Alvarez, M. M.; Wilkinson, A. *Acc*. *Chem*. *Res*. **1999,** *32,* 397-406.

(34) Brust, M.; Kiely, C. J. *Colloids Surf*. **2002,** *202,* 175-186.

(35) Brust, M.; Kiely, C. J. *Colloids and colloid assemblies;* Caruso, F., Ed.; Wiley-VCH: Weinheim, 2004; pp 96-119.

(36) Daniel, M. C.; Astruc, D. *Chem*. *ReV.* **2004,** *104,* 293-346.

(37) Wilson, R. *Chem*. *Commun*. **2003,** 108-109.

(38) Raphae, L.; Nguyen T. K. *J*. *AM*. *CHEM*. *SOC*. **2004,** 126, 10076-10084

(39) Lin, X. M.; Sorensen, C. M.; Klabunde, K. J. *J*. *Nanopart*. *Res*. **2000,** *2,* 154.

(40) Trivino, G.; Klabunde, K. J.; Dale, E. *Langmuir* **1987,** *3* (6), 986-992.

(41) (a) Lin, J.; Zhou, W.; O'Connor, C. J. *Mater. Lett*. **2001,** *49,* 282. (b) Zhou, Y.; Itoh, H.;

Uemura, T.; Naka, K.; Chujo, Y. *Langmuir* **2002,** *18,* 277. (c) Weare, W. W.; Reed, S. M.; Warner, M. G.; Hutchson, J. E. *J*. *Am*. *Chem*. *Soc*. **2000,** *122,* 12890.

(42) Marchetti. B.; Joseph. Y.; Bertagnolli. H. *J Nanopart Res* **2011,** 13, 3353–3362

(43) Kregig, U.&L. Genzel, 1985. Surface Sci. 156, 678-700

(44) Lin, X. M.; Jaeger, H. M.; Sorensen, C. M.; Klabunde, K. J. *J*. *Phys*. *Chem*. *B* **2001,** *105,* 3353.

(45) (a) Taleb, A.; Petit, C.; Pileni, M. P. *J*. *Phys*. *Chem*. *B* **1998,** *102,* 2214. (b) Storhoff, J. J.; Lazarides, A. A.; Mucic, R. C.; Mirkin, C. A.; Letsinger, R. L.; Schatz, G. C. *J*. *Am*. *Chem*. *Soc*. **2000,** *122,* 4640.

(46) Prasad, B. L. V.; Stoeva, S. I.; Sorensen, C. M.; Klabunde, K. J. *Langmuir* **2002,** *18,* 7515.

(47) Whitesides, G. M.; Love, J. C. *Sci*. *Am*. **2001,** *285,* 39.

(48) (a) Chikan, V.; Kelley, D. F. *J*. *Phys*. *Chem*. *B* **2002,** *106,* 3794. (b) Sugimoto, T. *Adv*. *Colloid Interface Sci*. **1987,** *28,* 65. Leff, D. V.; Ohara, P. C.; Heath, J. R.; Gelbart, W. M. *J*. *Phys*. *Chem*. **1995,** *99,* 7036.

(49) (a) Hamaker, H. C. *Physica* (Utrecht) **1937,** *4,* 1058. (b) Ohara, P. C.; Leff, D. V.; Heath, J. R.; Gelbart, W. M. *Phys*. *Rev*. *Lett*. **1995,** *75,* 3466.

(50) Stoeva, S. I.; Prasad, B. L. V.; Uma, S.; Stoimenov, P. K.; Sorensen, C. M.; Klabunde, K. J. *J*. *Phys*. *Chem*. *B* **2003,** *107, 7441* -7448

(51) Lin, X. M.; Wang, G. M.; Sorensen, C. M.; Klabunde, K. J. *J*. *Phys*. *Chem*. *B* **1999,** *103,* 5488-5492.

(52) Matthiesen, J.E.; Jose, D.; Sorensen, C. M.; Klabunde, K. J. J. Am. Chem. Soc. 2012, 134, 9376−9379